Preparation, Characterization, and Electrochemical Properties of Pure and Composite $LaNi_{0.6}Fe_{0.4}O_3$-Based Cathodes for IT-SOFC

Manuela Bevilacqua,[†] Tiziano Montini,[†] Claudio Tavagnacco,[†] Emiliano Fonda,[‡] Paolo Fornasiero,*[,†] and Mauro Graziani[†]

Chemistry Department and Centre of Excellence for Nanostructured Materials, University of Trieste and INSTM, Trieste, Italy, and Synchrotron SOLEIL L'Orme de Merisiers, St Aubin BP48, 91192 Gif sur Yvette Cedex, France

Received June 18, 2007. Revised Manuscript Received September 14, 2007

Recently $LaNi_{1-x}Fe_xO_3$ materials have been indicated as good candidates for cathodes for intermediate temperature solid oxide fuel cells (IT-SOFCs), and $LaNi_{0.6}Fe_{0.4}O_3$ (LNF) showed the highest specific conductivity in the $LaNi_{1-x}Fe_xO_3$ series. Here we report the results of our investigation on the performances of LNF, synthesized by the coprecipitation method. A detailed local structure analysis, performed using X-ray absorption near edge spectroscopy (XANES) and extended X-ray absorption fine structure (EXAFS) techniques, indicated that both Fe and Ni are in the (III) oxidation state with coordination numbers of ~6, suggesting the absence of appreciable amount of oxygen vacancies. The fresh LNF material was used as a precursor for LNF–YSZ (yttria-stabilized zirconia) and LNF–SDC (samaria-doped ceria) electrodes. In the case of the LNF–YSZ nanocomposite, even a short (5 h) treatment at 1000 °C induced a strong reaction between the cathode components, leading to the formation of an undesirable $La_2Zr_2O_7$ insulating layer. In the case of LNF–SDC, no evidences of reaction between the two components have been observed even at 1100 °C. Low area specific resistance (ASR) values were obtained by electrochemical impedance spectroscopy (EIS) for the composite LNF–SDC electrode in accordance with the good electronic conductivity of LNF and the high ionic conductivity of SDC. Pure LNF and composite LNF–SDC electrodes showed identical apparent activation energy, suggesting the presence of the same rate-determining step. However, ASR values for LNF–SDC were significantly smaller with respect to pure LNF. This is consistent with the hypothesis that the addition of SDC does not change the reaction mechanism, but it increases the triple phase boundary (TPB) length where the reaction occurs. Notably, the polarization of the electrode further improved the cathodic performance, increasing the number of active sites for the O_2 adsorption and activation.

1. Introduction

The promise of direct and efficient conversion of chemical to electrical energy makes fuel cell development an area of great technological interest. Solid oxide fuel cells (SOFCs) have the additional advantages of high efficiency, the ability to utilize high-temperature exhausts for cogeneration or hybrid applications, and the ability for internal reforming. SOFCs have been developed in both planar and tubular design configurations. An important consideration to both design and manufacturing research is the reduction of operating temperatures in order to reduce production costs.[1–3] The improvement of the electrode performance, especially on the cathodic side, is one of the most important subjects in the development of SOFCs.

A wide number of perovskitic materials have been investigated with the aim of improving the performances of the cathode.[1] $La_{(1-x)}Sr_xMnO_3$ (LSM) perovskite is one of the most investigated cathode material for high-temperature SOFCs because of its high thermal and chemical stability with YSZ electrolytes.[1,3] It has been observed that LSM reacts with YSZ above 1200–1300 °C depending on the Sr doping in the perovskite.[4–7] However, LSM is characterized by low ionic conductivity and relatively high activation energy for oxygen dissociation at temperatures below 800 °C.[3,8]

Several attempts have been made to use cobaltite-based cathodes. These materials are promising candidates for low-temperature SOFCs stacks because of the higher conductivity with respect to LSM. However, it has been suggested that, due to the large thermal expansion coefficient and their reactivity with zirconia,[1] Co-based electrodes should be preferably used with ceria electrolytes or in the presence of a protective layer of ceria to prevent the reaction with YSZ.

* Corresponding author: Tel + 39 040 558 3973; Fax + 39 040 558 3903 e-mail: pfornasiero@units.it.
[†] University of Trieste and INSTM.
[‡] Synchrotron SOLEIL L'Orme de Merisiers.

(1) Wincewicz, K. C.; Cooper, J. S. *J. Power Sources* **2005**, *140*, 280–296.
(2) McIntosh, S.; Gorte, R. J. *Chem. Rev.* **2004**, *104*, 4845–4865.
(3) Singhal, S. C.; Kendall, K. *High Temperature Solid Oxide Fuel Cells - Fundamentals, Design and Applications*; Elsevier Advanced Technology: Oxford, 2003.
(4) Hart, N. T.; Brandon, N. P.; Day, M. J.; Lapena-Rey, N. *J. Power Sources* **2002**, *106*, 42–50.
(5) van Roosmalen, J. A. M.; Cordfunke, E. H. P. *Solid State Ionics* **1992**, *52*, 303–312.
(6) Badwal, S. P. S. *Solid State Ionics* **2001**, *143*, 39–46.
(7) Mitterdorfer, A.; Gauckler, L. J. *Solid State Ionics* **1998**, *111*, 185–218.
(8) Murray, E. P.; Tsai, T.; Barnett, S. A. *Solid State Ionics* **1998**, *110*, 235–243.

10.1021/cm071622n CCC: $37.00
Published on Web 10/31/2007

Also, Sr-doped $LaFeO_3$ (LSF) materials exhibit superior performance as SOFCs cathode compared to LSM. However, in order to use these materials with YSZ-based cells, it is necessary to avoid contact with YSZ by incorporating an additional material (samaria- or gadolinia-doped ceria, SDC or GDC) as barrier between the cathode and the electrolyte. Another possibility is to use the impregnation method of porous YSZ matrix to fabricate composite electrode using treatments at lower temperature (below 1000 °C) to avoid the formation of the insulating species.[9]

$(La,Sr)(Co,Fe)O_{3-\delta}$ (LSCF) has been widely investigated as a promising cathode for IT-SOFCs, principally because of the mixed conductivity presented by these materials.[10–14] However, also in this case, the perovskite is not compatible with YSZ, and doped-CeO_2 electrolytes or interlayers must be used.

Recently, Chiba et al. investigated the effect of doping in Ni-based perovskitic materials, changing the doping cation in the B site of $LaNi_{0.6}M_{0.4}O_3$ (M = Al, Cr, Mn, Fe, Co, Ga) and the composition in the $LaNi_{1-x}Fe_xO_3$ ($x = 0.0$–1.0) series.[15] Also, the effect of different lanthanides or Y in the A site has been reported.[16] It has been suggested that $LaNi_{1-x}Fe_xO_3$ mixed oxides exhibit suitable properties as cathode materials for IT-SOFC, such as high electrical conductivity and thermal expansion coefficient closer than LSM to that of YSZ electrolyte.[15,17,18] $LaNi_{1-x}Fe_xO_3$ have been tested as cathodes in SOFCs with YSZ and SASZ (alumina-doped scandia-stabilized zirconia) although solid-state reaction with the electrolyte above 1000 °C results in the formation of a $La_2Zr_2O_7$ insulating layer.[19] Recently, the electrochemical properties of LNF–SDC composite electrodes combined with YSZ electrolyte have been investigated to evaluate the effect of the composite microstructure on the cell performance.[20]

We have already investigated the $LaNi_{0.6}Fe_{0.4}O_3$ material showing the importance of preparation method and morphological characteristics to obtain high electrical conductivity, mainly electronic.[21] Here we extended our previous studies on LNF cathode by characterization with X-ray absorption fine structure (XAFS) spectroscopy to obtain a detailed description of the local structure and the oxidation state of the cations in the B site of the perovskite. Furthermore, we evaluated the performances of $LaNi_{0.6}Fe_{0.4}O_3$ in symmetrical cells and its compatibility with YSZ and SDC electrolytes. Electrochemical impedance spectroscopy (EIS) investigations performed at open-circuit voltage (OCV) on symmetrical cells are reported and discussed.

2. Experimental Section

2.1. Preparation of the Samples. $LaNi_{0.6}Fe_{0.4}O_3$ sample was prepared using the coprecipitation route.[21] Briefly, stoichiometric amounts of $La(NO_3)_3 \cdot XH_2O$ (99.9% Aldrich, 38.10% La_2O_3), $Ni(NO_3)_2 \cdot 6H_2O$ (puriss. Fluka), and $Fe(NO_3)_3 \cdot 9H_2O$ (puriss. Fluka) were dissolved in water to obtain a 0.1 M solution (total moles of cations per liter of solution). The metallic cations solution was added dropwise to an excess of a 1.0 M water solution of tetramethylammonium hydroxide (TMAH, 25 wt % aqueous solution, Aldrich) under vigorous stirring. To ensure full precipitation of the mixed hydroxides, the amount of base was 4 times that required by the stoichiometry. A green-yellow precipitate was obtained, which was aged at room temperature for 1 h before being filtered with an ash-free paper filter. The gelatinous precipitate was suspended in water (10 g/L with respect to the final mixed oxide) and stirred overnight to remove the excess of base. Afterward, the precipitate was filtered, dried at 120 °C for 24 h, grounded in a mortar, and calcined at 700 °C for 5 h in a static oven. ICP-MS analyses of mother liquor from filtration confirmed complete precipitation of the cations.

2.2. Characterization. Powder XRD patterns of the samples after calcination at different temperatures were recorded with a computer-controlled Philips X'Pert diffractometer using Cu Kα radiation.

Morphology of the samples was examined with a Jeol 5400 LV scanning electron microscope (SEM), operating at 25 kV, and equipped with an EDAX Genesis 2000 microanalysis system.

Near edge (XANES) and extended (EXAFS) X-ray absorption spectra were collected at the XAFS beamline at the Elettra synchrotron facility in Trieste operating at 2.0 GeV and 150–300 mA. All spectra were recorded in transmission mode with a Si(311) double crystal monochromator and using ionization chambers as detectors. Third harmonic rejection was achieved by monochromator detuning and proper selection of the gas mixture in the ionization chambers; second harmonics are absent due to the extinction rule of the Si(311). The energy resolution is $\Delta E/E = 10^{-4}$, and the photon flux at the sample is 10^{10} photons s^{-1} (0.01% bw, 0.1 A). Angle/energy calibration has been checked by simultaneously measuring a Ni or Fe metal foil absorption spectrum between the second and the third ionization chamber. XANES spectra have been recorded with an energy sampling stem from 0.1 to 1 eV and an integration time of 2 s per point over the range 6700–7400 eV for the Fe K edge and 7900–8600 eV for the Ni K edge. EXAFS spectra have been recorded with an energy sampling stem from 2 to 5 eV, and an integration time of 2 s per point over the range 6700–8200 eV for the Fe K edge and 7900–9350 eV for the Ni K edge. Each EXAFS spectrum has been acquired three times for the signal-to-noise ratio optimization and for the error bars evaluation. EXAFS data analysis has been performed with IFeffit[22] and Feff 8.2.[23] S_0^2 has been tested on reference compounds and fixed to 0.9 for Fe and 0.76 for Ni K-edges. The coordination numbers for coordination shells beyond the first have not been varied in the fit; La atoms are

(9) Huang, Y. Y.; Vohs, J. M.; Gorte, R. J. *J. Electrochem. Soc.* **2004**, *151*, A646–A651.
(10) Esquirol, A.; Brandon, N. P.; Kilner, J. A.; Mogensen, M. *J. Electrochem. Soc.* **2004**, *151*, A1847–A1855.
(11) Esquirol, A.; Kilner, J.; Brandon, N. *Solid State Ionics* **2004**, *175*, 63–67.
(12) Kim, W. H.; Song, H. S.; Moon, J.; Lee, H. W. *Solid State Ionics* **2006**, *177*, 3211–3216.
(13) Murray, E. P.; Sever, M. J.; Barnett, S. A. *Solid State Ionics* **2002**, *148*, 27–34.
(14) Raj, I. A.; Nesaraj, A. S.; Kumar, M.; Tietz, F.; Buchkremer, H. P.; Stoever, D. *J. New Mater. Electrochem. Syst.* **2004**, *7*, 145–151.
(15) Chiba, R.; Yoshimura, F.; Sakurai, Y. *Solid State Ionics* **1999**, *124*, 281–288.
(16) Chiba, R.; Yoshimura, F.; Sakurai, Y. US6120924, 2000.
(17) Li, S.; Sun, X. L.; Wen, Z. S.; Sun, J. C. *Rare Met.* **2006**, *25*, 213–217.
(18) Basu, R. N.; Tietz, F.; Wessel, E.; Buchkremer, H. P.; Stover, D. *Mater. Res. Bull.* **2004**, *39*, 1335–1345.
(19) Orui, H.; Watanabe, K.; Chiba, R.; Arakawa, M. *J. Electrochem. Soc.* **2004**, *151*, A1412–A1417.
(20) Sornthummalee, P.; Sato, K.; Orui, H.; Chiba, R.; Arawaka, M. *Meet. Abstr.—Electrochem. Soc.* **2007**, *602*, 51.
(21) Bevilacqua, M.; Montini, T.; Tavagnacco, C.; Vicario, G.; Fornasiero, P.; Graziani, M. *Solid State Ionics* **2006**, *177*, 2957–2965.
(22) Newville, M. *J. Synchrotron Radiat.* **2001**, *8*, 322–324.
(23) Ankudinov, A. L.; Ravel, B.; Rehr, J. J.; Conradson, S. D. *Phys. Rev. B* **1998**, *58*, 7565–7576.

distributed over two distances around Fe or Ni, but since these distances cannot be resolved, their average has been refined in the fit procedure instead.

Symmetrical cells equipped with two-electrode configuration were used to perform EIS investigations. The effect of YSZ and SDC electrolyte materials has been considered. Different thicknesses for the electrolyte pellet have been evaluated, and the best treatment conditions (amount of powders, time of pressing, wt % of poly(vinyl alcohol) as organic binder) have been chosen to improve the compactness and geometrical regularity of disks. The best performance was obtained with electrolyte pellets prepared by pressing 0.450 g of 8 mol % Y_2O_3 + 92 mol % ZrO_2 powders (TZ-8Y, Tosoh) or cerium(IV) oxide–15% samaria-doped nanopowder (Aldrich), both mixed with 2 wt % of poly(vinyl alcohol) (Fluka), at 2 ton and sintering at 1500 °C for 5 h in air. The final result was a ceramic disk with thickness of ≈0.6 mm.

As-prepared $LaNi_{0.6}Fe_{0.4}O_3$ (LNF) powder was dispersed in β-citronellol (95%, Aldrich) as organic binder to obtain a paste easily applicable to the pellet surface by slurry coating. All the electrodes covered a geometric area of 0.23 cm^2. Two nominally identical electrodes were applied on each side of YSZ or SDC pellet and calcined at 1000 °C for 5 h in air. In this way, symmetrical cells with compositions LNF|YSZ|LNF and LNF|SDC|LNF have been prepared.

For symmetrical cells with LNF–YSZ and LNF–SDC composite electrodes, $LaNi_{0.6}Fe_{0.4}O_3$ powders were mixed with YSZ and SDC powders, respectively. Accordingly to previous studies for lanthanum (strontium) nickel iron mixed oxides (LSNF[24]) and for the same $LaNi_{0.6}Fe_{0.4}O_3$,[25] the composition of the composite cathode was chosen as 50 wt % LNF and 50 wt % YSZ or SDC.

For comparison and to check the experimental setup of the EIS measurements, symmetrical cells with pure $La_{0.8}Sr_{0.2}$ MnO_3 (LSM, Praxair Surface Technologies) electrodes have been prepared in the same way of LNF|YSZ|LNF and LNF|SDC|LNF.

Ag paste (silver conductive ink, Alfa Aesar) was used as current collector, accordingly to procedures previously reported by Gorte et al.[26–28] Prior to the measurements, each cell was held at a constant temperature of 800 °C for 20 h.

The electrode responses in the temperature range of 600–800 °C were measured using a Parstat 2273 instrument (PAR), with a small ac signal of 10 mV rms at zero dc polarization and over the frequency range of 100 mHz–300 kHz.

Apparent activation energies (E_a) for the oxygen reduction process at the electrodes and for O^{2-} ion conduction through the electrolyte have been obtained by temperature dependence at OCV.

The area specific resistance (ASR) for the electrodes has been calculated as the difference between the low- and the high-frequency intercepts at the real axis, multiplied by 0.5 to account for the two electrodes.

EIS results are reproducible, and each ASR and E_a value reported in this paper is the mean value of at least three measurements.

Complex impedance measurements after polarization treatment were carried out using a thick three-electrode test cell. The counter and the working electrodes were nominally identical. The Ag wire reference electrode was wrapped around the outside. A current density of 250 mA cm^{-2} was applied for 10 min to polarize the cell, as was reported by Gorte and co-workers[29] with conventional LSM–YSZ electrodes. In our case, no further modifications were observed for longer polarization treatments (up to 1 h).

Analysis of the impedance spectra was made using the software Zview (Scribner Associates, Inc.). Data were fitted to equivalent circuits to determine the electrolyte and overpotential resistances. It is known that the equivalent circuit approach leaves the electrode reaction mechanism vaguely or empirically defined, with poor connection between fitted parameters and the properties of the investigated material.[30] However, the simple model used to fit the data may provide a useful set of parameters to discriminate the limiting step of the cathodic process.

3. Results and Discussion

3.1. Local Structure of $LaNi_{0.6}Fe_{0.4}O_3$. The $LaNi_{0.6}Fe_{0.4}O_3$ has been previously reported as material with a high electronic conductivity[15,18] that appears to be strongly influenced by the preparation route.[18,21] Moreover, the increase of the calcination temperature leads to higher conductivity.[21] Besides densification of the material, the formation of defects, as a result of the high-temperature treatments, can be responsible for the improved performances. In an attempt to verify this hypothesis, XAFS experiments have been performed.

Figure 1 reports the XANES spectra at the Fe and Ni K-edges recorded on the $LaNi_{0.6}Fe_{0.4}O_3$ after calcination at different temperatures. The obtained spectra are very similar, and no significant differences have been observed also analyzing the first-derivative spectra (data not shown). These results suggest that the oxidation state and the local symmetry around the cations hosted in the B site of the $LaNi_{0.6}Fe_{0.4}O_3$ perovskite are not appreciably influenced by the applied thermal treatments. Furthermore, the XANES spectra at the Ni K-edge are very similar to that obtained for a reference homogeneous $LaNiO_3$ sample (prepared by precipitation with TMAH and calcination at 700 °C) and to those reported in the literature for the same material.[31,32] The band in the pre-edge region at 8334.2 eV is assignable to the $1s \rightarrow T_{1u}$ transition, where T_{1u} is the oxygen p band of the right symmetry in the $3d^8\underline{L}$ configuration.[31] The main absorption peak at 8350.0 e$\overline{V}$ is schematically assignable to the $1s \rightarrow 4p$ transition,[32] but two components are present; Garcia et al. suggested that the fundamental state of the Ni ion is a mixed electronic configuration between $3d^7$ and $3d^8\underline{L}$.[31] The $3d^8\underline{L}$ configuration represents a situation with a c$\overline{h}$arge transfe$\overline{r}$ mechanism active between Ni^{3+} and its nearest neighbours, the O^{2-} ions. Fitting $LaNiO_3$ XANES, Garcia et al. found that the ground state is composed of 40% of $3d^8$ and 60% of $3d^8\underline{L}$ configurations.[31] Spectra recorded at the Ni K-edge sugge$\overline{s}$t that the electronic configuration of the Ni ion in the $LaNi_{0.6}Fe_{0.4}O_3$ materials reported here is very similar to that present in the $LaNiO_3$ reference,

(24) Zhu, G. Y.; Fang, X. H.; Xia, C. R.; Liu, X. Q. *Ceram. Int.* **2005**, *31*, 115–119.
(25) Li, S.; Sun, J. C.; Sun, X. L.; Zhu, B. *Electrochem. Solid State Lett.* **2006**, *9*, A86–A87.
(26) Huang, Y. Y.; Ahn, K.; Vohs, J. M.; Gorte, R. J. *J. Electrochem. Soc.* **2004**, *151*, A1592–A1597.
(27) Huang, Y.; Vohs, J. M.; Gorte, R. J. *J. Electrochem. Soc.* **2006**, *153* (6), A951–A955.
(28) McIntosh, S.; Adler, S. B.; Vohs, J. M.; Gorte, R. J. *Electrochem. Solid State Lett.* **2004**, *7*, A111–A114.
(29) Huang, Y. Y.; Vohs, J. M.; Gorte, R. J. *J. Electrochem. Soc.* **2005**, *152*, A1347–A1353.
(30) Adler, S. B. *Solid State Ionics* **1998**, *111*, 125–134.
(31) Garcia, J.; Blasco, J.; Proietti, M. G.; Benfatto, M. *Phys. Rev. B* **1995**, *52*, 15823–15828.
(32) Park, J. C.; Kim, D. K.; Byeon, S. H.; Kim, D. *J. Synchrotron Radiat.* **2001**, *8*, 704–706.

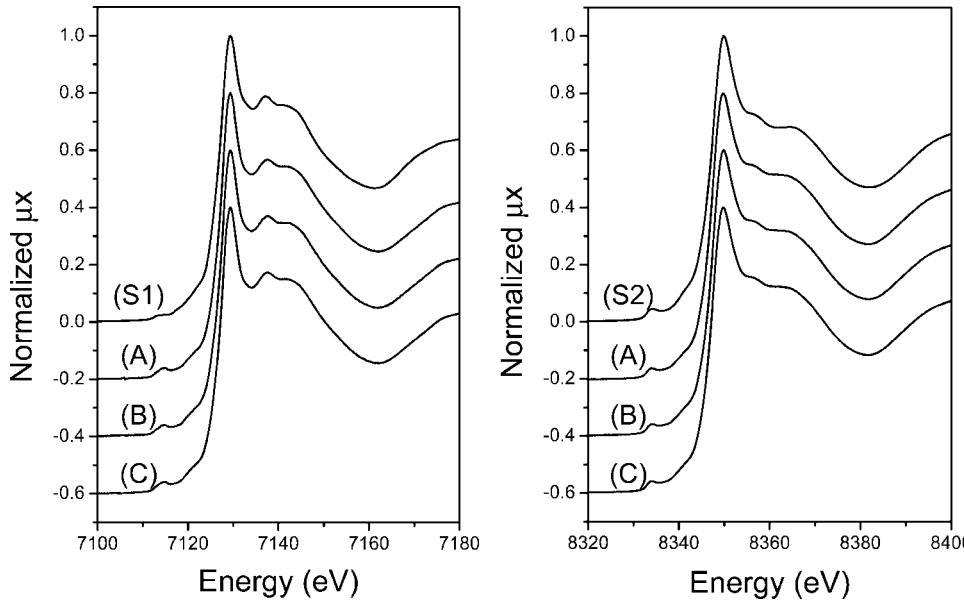

Figure 1. XANES spectra at the Fe K-edge (left part) and at the Ni K-edge (right part) of the $LaNi_{0.6}Fe_{0.4}O_3$ materials after calcination for 5 h at (A) 1000, (B) 1100, and (C) 1200 °C. The XANES spectra of standard $LaFeO_3$ (S1) and $LaNiO_3$ (S2) are reported for comparison.

and the charge transfer could explain the black color of the powders. The XANES spectra at the Fe K-edge are not modified by the calcination temperature up to 1200 °C and are in good agreement with that of a homogeneous $LaFeO_3$ sample (prepared by precipitation with Na_2CO_3 and calcination at 1000 °C) and to those previously reported for $LaFeO_3$,[33] indicating that the iron is present in the Fe(III) state. The absorption band present in the pre-edge region at 7114.9 eV is assignable to the 1s → 3d transition. Formally, this dipolar transition is Laporte-forbidden, but it gains intensity through coupling mechanism or p–d hybridization, when the iron center is in a noncentrosymmetrically environment.[34] This band in our $LaNi_{0.6}Fe_{0.4}O_3$ samples appears more intense with respect to the previously reported $LaFeO_3$.[33] This fact suggests that the site which hosts the Fe(III) in the $LaNi_{0.6}Fe_{0.4}O_3$ is not perfectly centrosymmetric, as attempted for a $3d^5$ ion in an octahedral site. This distortion can be induced by the presence of Ni(III), which determines the structure of the material (rhombohedral as $LaNiO_3$ instead of the orthorombic structure of $LaFeO_3$).

EXAFS spectra, extracted from the data recorded at the Fe and Ni K-edges on the LNF sample calcined at 1000 °C, are shown in Figures 2 and 3. The simulations confirm the hypothesis that the structure is not significantly different from the rhombohedral crystallographic model of $LaNi_{0.6}Fe_{0.4}O_3$ reported by Falcon et al.[35]

Fe and Ni cannot be distinguished by their scattering factors. Fe–Fe and Fe–Ni distances for Fe K-edge and Ni–Fe and Ni–Ni distances for Ni K-edge EXAFS are supposed to be identical in our simulation, and this turns out to be a good approximation. The refinement includes the first, second, and third coordination shells and the most important multiple

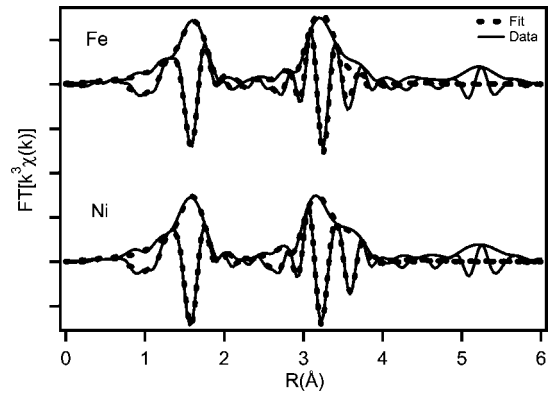

Figure 2. Fe and Ni K-edge EXAFS signals and their fits with theoretical standards.

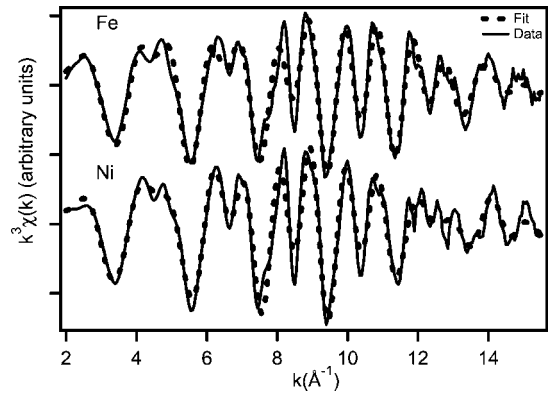

Figure 3. Envelopes and imaginary parts of the experimental and simulated EXAFS signals at the Fe and Ni K-edges.

scattering paths involving quasi-collinear M–O–M (M = Fe, Ni) arrangements. These paths depend on the M–O–M angle that in the model is 163.4°; to better fit data and obtain an estimate of the angle, we used a combination of two paths

(33) Berry, F. J.; Gancedo, J. R.; Marco, J. F.; Ren, X. L. *J. Solid State Chem.* **2004**, *177*, 2101–2114.
(34) Wong, S. T.; Lee, J. F.; Cheng, S. F.; Mou, C. Y. *Appl. Catal., A* **2000**, *198*, 115–126.
(35) Falcon, H.; Goeta, A. E.; Punte, G.; Carbonio, R. E. *J. Solid State Chem.* **1997**, *133*, 379–385.

Table 1. EXAFS Data Fitting Parameters: Coordination Number (CN), Distances, and Debye–Waller Factors σ

CN	bond	distance (nm)	σ (nm^2)
5.9 ± 0.6	Fe–O	0.1969 ± 0.0001	$(4.5 \pm 0.8) \times 10^{-5}$
6	Fe–La	0.3378 ± 0.0006	$(7.5 \pm 0.4) \times 10^{-5}$
6	Fe–Ni,Fe	0.389 ± 0.001	$(4.8 \pm 0.7) \times 10^{-5}$
6.3 ± 0.4	Ni–O	0.1943 ± 0.0004	$(3.9 \pm 0.4) \times 10^{-5}$
6	Ni–La	0.3334 ± 0.0004	$(7.4 \pm 0.3) \times 10^{-5}$
6	Ni–Ni,Fe	0.3859 ± 0.0008	$(7.7 \pm 0.8) \times 10^{-5}$

calculated for 170° and 160°. Larger angles (quasi-collinear M–O–M arrangements) have been tested, too.

Numerical results concerning Ni and Fe local structures are summarized in Table 1; distances around Ni appear all shorter with respect to those around Fe, while the model determined by XRD on a similar materials[35] is intermediate, suggesting to be an average of the different Fe and Ni sites that cannot be distinguished by diffraction. Angles can be determined, too, deduced by distances or directly by fit. The average of Ni–O–M and Fe–O–M angles (M = Ni, Fe) is 163°, which matches the XRD model. Falcon et al.[35] indicated how the normalized cell volume (*V*/*Z*) increases linearly with the iron content due to the larger radius of Fe(III) (HS) compared to Ni(III) (LS). Our findings are in agreement, and they independently probe the Fe and Ni local structures that, apart from a difference of about 1% in distances and 2% in angles, are very similar.

The coordination numbers deduced by the EXAFS fits are very close to 6, which is the theoretical coordination number of the cations hosted in the B site of a perovskitic material. This fact suggests that a negligible amount of oxygen vacancies is present in the structure of the material. In fact, the presence of an appreciable number of oxygen vacancies would result in a significant reduction of the coordination number of Fe and/or Ni and in the decrease of their oxidation state. The absence of oxygen vacancies is also in agreement with the electrical conductivity measurement previously reported,[21] which evidenced a low activation energy consistently with a small polaron conductive mechanism.

3.2. Compatibility between $LaNi_{0.6}Fe_{0.4}O_3$ and the Electrolytes. Lanthanum-based perovskites have been previously reported to react at high temperature with zirconia-based electrolytes leading to the formation of $La_2Zr_2O_7$, with detrimental effects on the electrical conductivity and the cathode performance. The chemical compatibility between $La_{0.99}(Ni_{0.59}Fe_{0.41})O_{3-\delta}$ cathode and $Zr_{0.85}Y_{0.15}O_{1.925}$ electrolyte was studied by Knudsen et al.[36] They found that just after 2 h of calcinations at 1125 °C the majority of La reacted with zirconia to form $La_2Zr_2O_7$. Moreover, Orui et al.[37] reported that, using an alumina-doped scandia-stabilized zirconia electrolyte, a layer of insulating $La_2Zr_2O_7$ was formed at the cathode/electrolyte interface after pretreatments at temperatures higher than 1000 °C. Consistently, our XRD data (not reported) confirm that the 50 wt % LNF–50 wt % YSZ composite cathode, coated on the surface of a YSZ pellet and sintered at 1000 °C for 5 h, showed the initial formation of $La_2Zr_2O_7$ while $LaNi_{0.6}Fe_{0.4}O_3$ was still present. After prolonged aging at 1000 °C (up to 70 h), XRD patterns of $La_2Zr_2O_7$ were well-developed. For this reason SDC was investigated as an alternative electrolyte to YSZ. In fact, it has been suggested that, compared with YSZ, ceria-based electrolytes have less reactivity with perovskite materials containing La and Sr.[3] This can be associated with the lower acidic nature of CeO_2 with respect to ZrO_2. Furthermore, compared with Zr(IV) ions, Ce(IV) ions are too big to form perovskites with La and Sr.[3] Symmetrical cells with pure $LaNi_{0.6}Fe_{0.4}O_3$ coated on a SDC pellet and calcined at 1000 °C for a long time (70 h) showed a XRD profile typical of a physical mixture of $LaNi_{0.6}Fe_{0.4}O_3$ (rhombohedral structure; space group $R\bar{3}c$)[35] and SDC (Figure 4, trace B). In the case of the composite cathode (50 wt % of $LaNi_{0.6}Fe_{0.4}O_3$ + 50 wt % of SDC) no evidences of insulating phases were found after calcinations at 1000 °C for 5 h (Figure 4, trace C) and even after calcinations at 1100 °C for 10 h (Figure 4, trace D).

Figure 5 shows representative SEM micrographs of LNF–SDC|SDC|LNF–SDC symmetric cells. Notably that, despite the high calcinations temperature (1500 °C), the SDC electrolyte is characterized by an appreciable porosity, which, however, does not significantly affect its ionic conductivity (values coincident with literature data;[3] see below). The thickness of the LNF–SDC composite layer varies between 5 and 30 μm. All the observed micrographs show that the LNF–SDC composite layer maintains a good porosity, useful for the diffusion and activation of the O_2 molecules. EDX analysis excludes the occurrence of appreciable phenomena of metal ion migration/diffusion even after calcinations at 1100 °C for 10 h (Figure 5, part B), confirming the absence of other phases resulting form the reaction between SDC and LNF. An 8–12 μm homogeneous Ag layer is present in the tested cell (Figure 5, part C). It was previously suggested that the use of Ag paste can have detrimental effects on the performance of the electrode due to the diffusion of Ag to the electrolyte–electrode interface.[38] Our SEM micrographs indicate the absence of significant Ag diffusion as a result of the application of the Ag paste on the composite electrode previously sintered at relatively high temperature, as reported by other authors.[39]

In summary, the present structural and morphological data confirmed that $LaNi_{0.6}Fe_{0.4}O_3$ can undergo a diffuse solid state reaction with zirconia-based electrolyte. In particular, when a composite cathode was used to extend the TPB, the perovskitic material easily formed an undesirable insulating layer of $La_2Zr_2O_7$. On the other hand, when a ceria-based electrolyte was used, no solid-state reaction with $LaNi_{0.6}Fe_{0.4}O_3$ was observed. These results suggest that, in the case of LNF, a ceria-based oxide interlayer could be used to prevent the reaction between LNF and an YSZ electrolyte, as reported for other cathode materials.[1,3]

3.3. Impedance Spectroscopy Characterization. Before discussing the present impedance spectroscopy characteriza-

(36) Knudsen, J.; Friehling, P. B.; Bonanos, N. *Solid State Ionics* **2005**, *176*, 1563–1569.
(37) Tabata, Y.; Orui, H.; Watanabe, K.; Chiba, R.; Arakawa, M.; Yamazaki, Y. *J. Electrochem. Soc.* **2004**, *151*, A418–A421.
(38) Simner, S. P.; Anderson, M. D.; Pederson, L. R.; Stevenson, J. W. *J. Electrochem. Soc.* **2005**, *152*, A1851–A1859.
(39) Wang, W.; Gross, M. D.; Vohs, J. M.; Gorte, R. J. *J. Electrochem. Soc.* **2007**, *154*, 439–445.

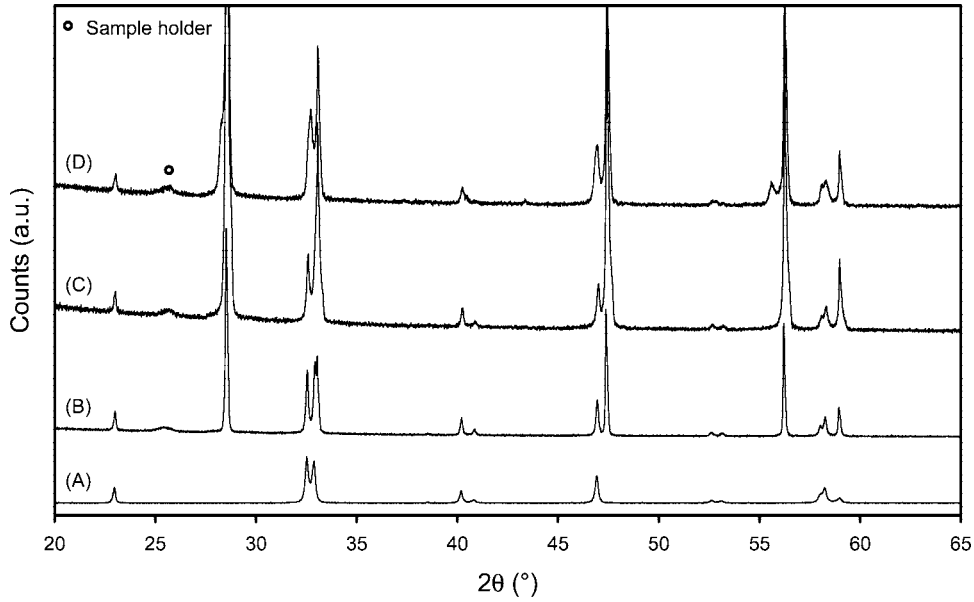

Figure 4. Powder XRD patterns of (A) LNF sample after 5 h of calcination at 1000 °C, (B) LNF|SDC|LNF after 70 h of calcination at 1000 °C, (C) LNF–SDC|SDC|LNF–SDC after 5 h of calcination at 1000 °C, and (D) LNF–SDC|SDC|LNF–SDC after 10 h of calcination at 1100 °C.

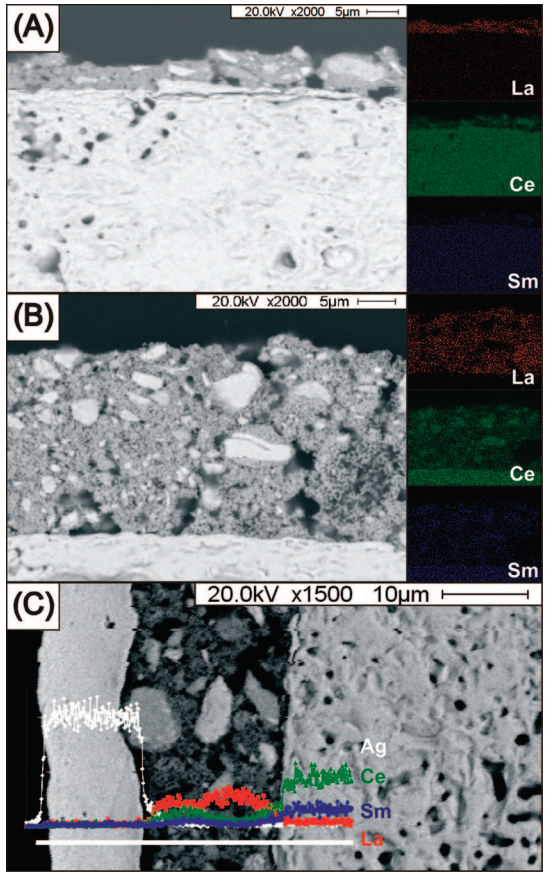

Figure 5. Representative SEM micrographs of (A) LNF–SDC|SDC|LNF–SDC after calcination at 1000 °C for 5 h, (B) LNF–SDC|SDC|LNF–SDC after calcination at 1100 °C for 10 h and (C) LNF–SDC|SDC|LNF–SDC calcined at 1000 °C after impedance tests up to 800 °C (with Ag ink).

tion, it is important to highlight that the accuracy of the impedance measurements are significantly influenced by the cell configuration.[40] The characterization of an electrode can be performed on a three-electrode cells, equipped with working electrode, WE, counter electrode, CE, and reference electrode, RE. This configuration offers great flexibility, but it is also susceptible to subtle errors due to the relative positioning of the RE in respect to the WE. Two-electrode symmetrical arrangements have been often adopted to minimize this inconvenience.[40] Furthermore, it was previously reported that the polarization resistance of the present materials increases with time without a significant change of the ohmic resistance.[21] Therefore, prior to our measurements each cell was hold at constant temperature of 800 °C for 20 h to obtain constant/stable Nyquist plots.

The interpretation of EIS measurement for a symmetrical two-electrode setup is complex. According to Adler,[30] the impedance of a symmetrical cell, recorded at OCV, can be expressed as the sum of charge-transfer resistances and impedances, plus a "chemical" impedance associated with non-charge-transfer processes. The contribution at intermediate/high frequencies is related essentially to electron transfer and ion transfer at the current collector/electrode and electrode/electrolyte interfaces, respectively, while the contribution at low frequencies can be associated with non-charge-transfer processes (including oxygen surface exchange, solid-state diffusion, and gas-phase diffusion inside and outside the electrode).[30]

Two simple circuits have been used to fit the experimental data from EIS measurements, and they are reported in Scheme 1. In each circuit, a resistance has been introduced to account for the electrolyte (R_{EL}) while an impedance (made by a resistance, R, in parallel with a constant phase element, CPE) has been introduced for each charge-transfer and diffusional processes. The EC1 circuit was used when diffusional processes are negligible. (The impedance element which accounts for the diffusional processes is missing.) This approach gives us the possibility to obtain and discuss their role by the comparison of overpotential resistances. In every analysis the area specific resistance of the electrolyte well

(40) Barsoukov, E.; Ross Macdonald, J. *Impedance Spectroscopy*; Wiley-Interscience: New York, 2005.

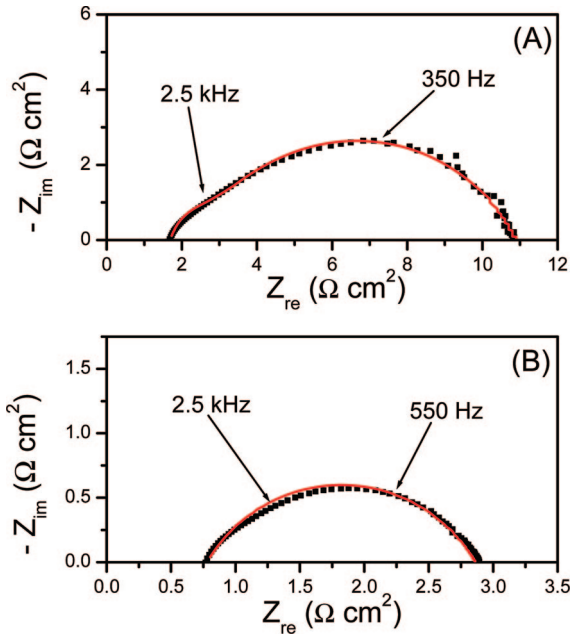

Figure 6. Nyquist plots of two-electrode symmetric cells measured at 800 °C: (A) LNF|YSZ|LNF and (B) LNF|SDC|LNF. Red lines: simulated Nyquist plot resulting from the equivalent circuit analysis using EC2 circuit for part A and EC1 circuit for part B.

agrees with the experimental measurement. In the Nyquist plots, it is reported the fitting results from the equivalent circuit that better fit the experimental data.

3.3.1. LNF Electrode on YSZ and SDC Electrolyte. Complex impedance measurements on the pure LNF electrode on both YSZ and SDC electrolyte have been collected every 25 °C in the temperature range 600–800 °C. Figure 6 shows representative Nyquist plots taken at 800 °C in air for LNF electrodes on YSZ (part A) and on SDC (Part B) electrolytes, respectively.

The data for LNF|YSZ|LNF symmetrical cells showed depressed arcs which are dominated by processes with frequencies in the range of 300–400 Hz, likely affected by different contributions.[29] The experimental data were fitted using the EC2 circuit. The analysis of area specific resistance values showed a dominant effect due to charge-transfer processes ($R_{CT} = 4.2\ \Omega\ cm^{-1}$) with a minor contribute due to diffusional processes ($R_{DIFF} = 0.4\ \Omega\ cm^{-1}$).

The ohmic resistance of the YSZ electrolyte at 700 °C was comparable with that predictable for a 600 μm electrolyte pellet, assuming a conductivity of 0.021 S cm^{-1}.[29,41] ASR mean value for the LNF|YSZ|LNF symmetrical cells was 4.6 $\Omega\ cm^2$ at 800 °C.

In the case of LNF|SDC|LNF symmetrical cells, depressed arcs were also observed, but they were dominated by processes with a frequency in the range of 500–600 Hz. The experimental data were fitted using the EC1 circuit, which shows mainly the semicircle at intermediate/high frequencies. Consequently, the estimated area specific resistance due to charge-transfer processes is equal to the total overpotential, without a considerable contribution of the diffusional processes. The ohmic resistances for SDC electrolytes corresponded to a conductivity of 0.038 S cm^{-1} at 700 °C and

Scheme 1

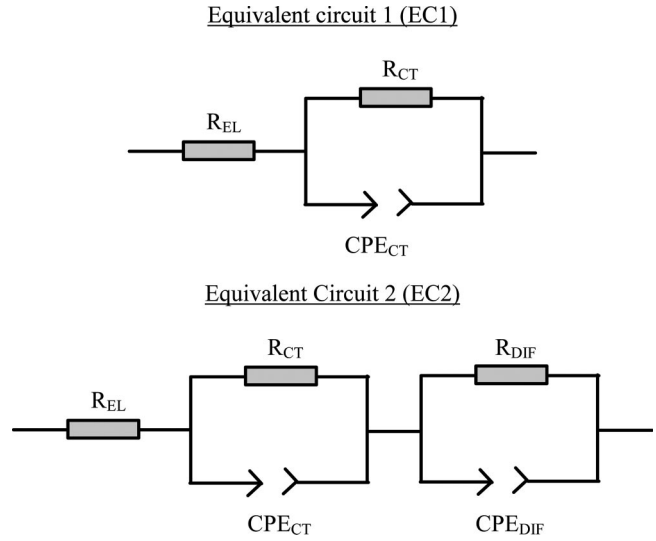

0.075 S cm^{-1} at 800 °C, which are in good agreement with that expected from the literature.[3,42–44] The ASR mean value of LNF|SDC|LNF symmetrical cells was determined to be 1.3 $\Omega\ cm^2$ at 800 °C.

Figure 7, parts A and B, shows the temperature dependence of ASR for LNF electrode on YSZ and SDC electrolytes. From these data, apparent activation energies (E_a) for the oxygen reduction process of 118 and 133 kJ mol^{-1} were determined for the LNF|YSZ|LNF half-cells and for the LNF|SDC|LNF half-cells, respectively. For similar half-cells prepared with commercial LSM, E_a values of 154 and 165 kJ mol^{-1} were obtained using YSZ and SDC electrolytes (data reported in Figure 7, parts C and D, respectively). The latter values well agree with that previously reported for similar systems,[8,45] indicating a good reproducibility of our electrochemical characterization setup with respect to the data reported in the literature and validating our measurement procedure. Moreover, E_a results for our LNF|SDC|LNF half-cells are in good agreement with those obtained for similar Ni/Fe-based perovskites, as pure cathode materials evaluated in the range of temperature 500–850 °C, such as $La_{0.4}Sr_{0.6}Ni_{0.2}Fe_{0.8}O_3$.[24]

The E_a calculated for the cathodic process and the frequency related to the main arc in the Nyquist plots would suggest that LNF-based systems have a similar rate-determining step with respect to that attributed to LSM cathode. For this latter system, previous studies on the dependence of the impedance spectra with p_{O_2} accompanied by a high activation energy, suggested that the limiting reaction step involves both oxygen dissociation and adsorption.[8,46,47] Although the activation energy observed for LNF-based symmetrical cells is lower than that observed for the LSM-based ones, the calculated value

(41) Sasaki, K.; Maier, J. *Solid State Ionics* **2000**, *134*, 303–321.
(42) Yahiro, H.; Eguchi, Y.; Eguchi, K.; Arai, H. *J. Appl. Electrochem.* **1988**, *18*, 527–531.
(43) Jung, G. B.; Huang, T. J. *J. Mater. Sci.* **2003**, *38*, 2461–2468.
(44) Wang, F. Y.; Chen, S. Y.; Cheng, S. *Electrochem. Commun.* **2004**, *6*, 743–746.
(45) Xu, X. Y.; Jiang, Z. Y.; Fan, X.; Xia, C. R. *Solid State Ionics* **2006**, *177*, 2113–2117.

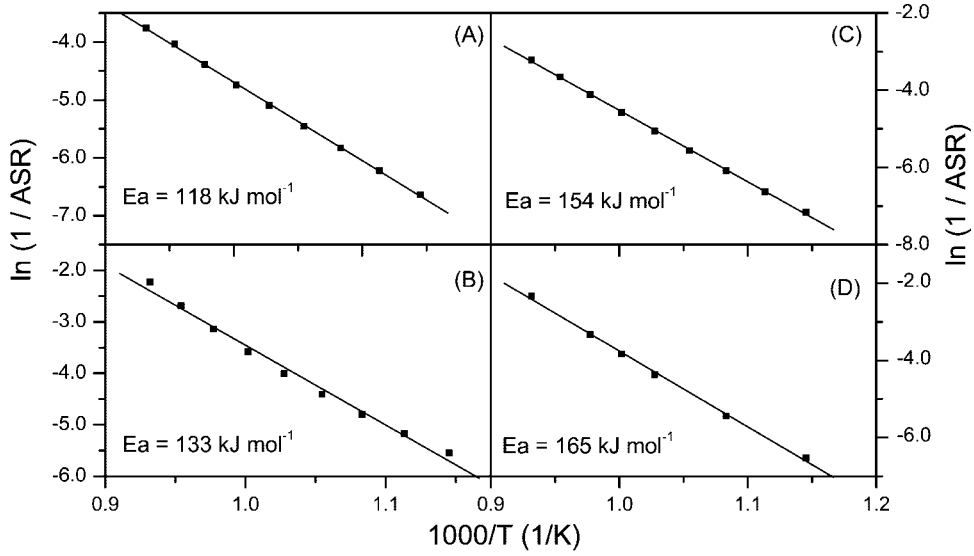

Figure 7. Arrhenius plots for (A) LNF|YSZ|LNF, (B) LNF|SDC|LNF, (C) LSM|YSZ|LSM, and (D) LSM|SDC|LSM.

was still high enough to be related to the activation of O_2 and the transport of O^{2-} ions. This hypothesis is also in agreement with the main results obtained by EXAFS measurements. In fact, the absence of oxygen vacancies represents a detrimental situation for the activation of O_2 on the TPB and/or the transport of O^{2-} ions through the electrode.

Finally, an apparent activation energy for O^{2-} ion conduction process at YSZ electrolyte of LNF|YSZ|LNF half-cells (90–95 kJ mol^{-1}) and SDC electrolyte of LNF|SDC|LNF half-cells (67–72 kJ mol^{-1}) were calculated from Arrhenius plots. The obtained values are in good agreement with those reported in the literature.[3,48,49] This confirms the correct experimental setup.

3.3.2. LNF–YSZ and LNF–SDC Composite Electrodes. Figure 8 shows representative Nyquist plots taken at 700 and 800 °C in air for LNF–YSZ electrodes on YSZ electrolyte. Unlike pure LNF, in the case of LNF–YSZ composite electrodes the ohmic resistance was higher than the value expected for a 600 μm electrolyte, assuming a conductivity of 0.021 S cm^{-1} at 700 °C for YSZ. Moreover, ASR values for LNF–YSZ composite electrodes were higher than those obtained for pure LNF electrodes. This was an indirect indication that a reaction between the electrode and the electrolyte materials takes place at the interface, leading to the formation of an insulating layer (see XRD data). The impedance data were fitted using the EC2 circuit, but the goodness of fit was very low, so a reasonable evaluation of fit parameters was not possible. This can be reasonably attributed to the complexity of the system resulting from solid-state reaction between LNF and YSZ.

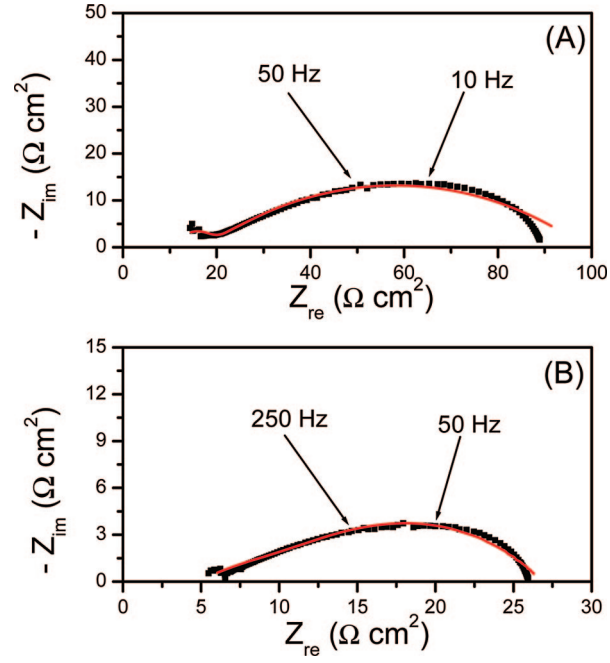

Figure 8. Nyquist plots of two-electrode symmetric LNF–YSZ|YSZ|LNF–YSZ cell measured at (A) 700 and (B) 800 °C. Red lines: simulated Nyquist plot resulting from the equivalent circuit analysis using EC2 circuit.

Unlike the LNF–YSZ composite electrode, the LNF–SDC composite system showed improved performances with respect to the pure electrodes. The ohmic resistances corresponding to conductivities of 0.039 S cm^{-1} at 700 °C and 0.075 S cm^{-1} at 800 °C also in this case were in good agreement with that expected for SDC electrolytes[3] and confirmed that no passivating species were formed at the interface between LNF and SDC. The calculated ASR mean values were 0.48 and 2.8 Ω cm^2 at 800 and 700 °C, respectively, much lower than those obtained for a pure LNF electrode. The activation energy for the cathodic process on the LNF–SDC composite electrode was calculated around 136 kJ mol^{-1}, very similar to the case of a pure LNF electrode. However, the polarization resistance of LNF–SDC electrode (with composition 50

(46) Barbucci, A.; Carpanese, P.; Cerisola, G.; Viviani, M. *Solid State Ionics* **2005**, *176*, 1753–1758.
(47) Vanherle, J.; Mcevoy, A. J.; Thampi, K. R. *Electrochim. Acta* **1996**, *41*, 1447–1454.
(48) Yang, C. C. T.; Wei, W. C. J.; Roosen, A. *Mater. Chem. Phys.* **2003**, *81*, 134–142.
(49) Mori, T.; Wang, Y. R.; Drennan, J.; Auchterlonie, G.; Li, J. G.; Ikegami, T. *Solid State Ionics* **2004**, *175*, 641–649.

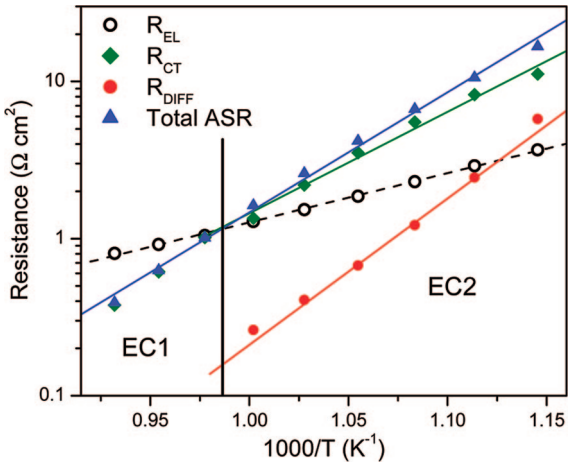

Figure 9. Area-specific resistances of the composite LNF–SDC symmetrical cells between 600 and 800 °C. ASR values are determined from the amplitude for the Nyquist plots. R_{EL}, R_{CT}, and R_{DIFF} are obtained from the equivalent circuit analysis using the indicated circuits.

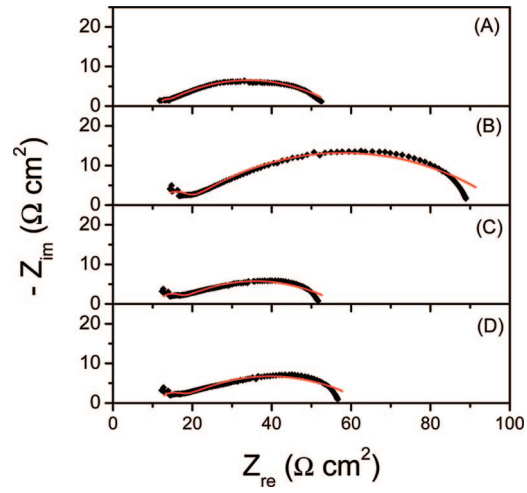

Figure 10. Nyquist plots at 700 °C on a two-electrode symmetric LNF–YSZ|YSZ|LNF–YSZ cell: effect of polarization (250 mA cm^{-2}, 10 min, 700 °C): (A) fresh cell; (B) cell aged at 800 °C for 20 h; (C) cell after aging at 800 °C 20 h and polarization; (D) after 5 h after the polarization. Red lines: simulated Nyquist plot resulting from the equivalent circuit analysis using EC2 circuit.

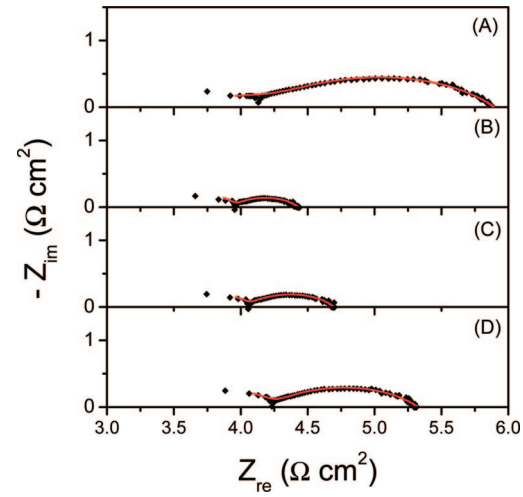

Figure 11. Nyquist plots at 700 °C on a three-electrode symmetric LNF–SDC|SDC|LNF–SDC cell: activation effect of polarization (250 mA cm^{-2} for 10 min at 700 °C): (A) cell aged at 800 °C 20 h, (B) cell aged at 800 °C 20 h immediately after the polarization, (C) after 5 h from the polarization, and (D) after 150 h from the polarization. Red lines: simulated Nyquist plot resulting from the equivalent circuit analysis using EC2 circuit.

wt % LNF + 50 wt % SDC) was lower than 50% with respect to the pure LNF at any temperature investigated. This is consistent with the idea that addition of SDC does not change the reaction mechanism and the rate determining of the electrodic process: the increase in the electrodic performances could be related to the increase of the TPB length.[8] Despite this hypothesis, some changes were observed on the frequencies of the main arcs recorded in the Nyquist plots increasing the temperature. Figure 9 shows the area specific resistances for the LNF–SDC composite symmetrical cell determined from the impedance spectra. The data were fitted using EC2 circuit between 600 and 725 °C while at higher temperature a better fit was obtained using EC1 circuit. A relatively large overpotential contribution (but not dominant) from non-charge-transfer processes is observed at low temperature (600–650 °C). It decreases increasing the temperature and above 750 °C the total area specific resistance corresponds to the pure charge-transfer contribution.

3.3.3. Activation Effect of the Polarization on Symmetric Cells. The impedance spectra of all the LNF-based systems at OCV, taken immediately after passing current through a two-electrode symmetric cell, were different from the corresponding spectra taken prior to polarize the cell. A dramatic decrease in the electrode impedances was always observed, indicating the occurrence of both anodic and cathodic polarization. For instance, the impedance spectrum of the composite LNF–YSZ, collected at 700 °C in a two-electrode symmetric cell, after polarization at 250 mA cm^{-2} was similar to that obtained on a fresh cell not exposed to aging (800 °C for 20 h) (Figure 10). At OCV and at 700 °C, the ASR values obtained by the Nyquist plot increased with time. After 150 h it did not reach the original shape and values before polarization. Appling a second polarization treatment 150 h after the first one, a comparable promotional effect has been observed. As revealed by XRD, some insulating $La_2Zr_2O_7$ is formed during the initial calcination. The present investigation revealed that, during the long-term aging of the cell after polarization (150 h at 700 °C), further insulating species are not formed. Consistently similar results were obtained also for LNF– SDC two-electrodes symmetric cells. Moreover, the equivalent circuit analysis is reported without the discussion of the parameters resulting from the fit because of the area specific resistances recorded after polarization account for both the anodic and cathodic contributions. For this reason overpotential values cannot be simply divided by two and compared with those obtained before polarization.

Selected experiments on a three-electrode symmetric cell with composite LNF–SDC electrodes on SDC electrolyte were performed to discriminate the contribution of the anodic and the cathodic polarization (Figure 11). The activation effect of cathodic polarization showed the decrease of ASR value from about 2.0 to 0.5 Ω cm^2 at

700 °C (Figure 11). However, the activation after polarization was progressively lost over time, suggesting that a deactivation process occurred on the activated electrode. The peak frequency in the impedance spectra after polarization (Figure 11, part B) was around 2.5 kHz and moved to lower values (650/700 Hz) during deactivation (Figure 11, part D). After polarization, the ASR progressive increase is observed, although a complete loss of the promotional effect induced by the polarization is not reached also after 150 h at 700 °C. From the equivalent circuit analysis reported in Figure 11, a decrease of both area specific resistances due to charge-transfer phenomena (from $R_{CT} = 1.5\ \Omega\ cm^{-1}$ to $R_{CT} = 0.4\ \Omega\ cm^{-1}$) and diffusional processes (from $R_{DIFF} = 0.4\ \Omega\ cm^{-1}$ to $R_{DIFF} = 0.2\ \Omega\ cm^{-1}$) is observed after polarization, and their slow increase appears during deactivation.

Regarding impedance spectroscopy characterization of cathodic materials, Gorte and co-workers have recently highlighted that, when an electrode material is characterized by nonlinear and/or hysteretic behavior under polarization, the impedance determined in a normal fuel cell has low correspondence to that observed using symmetric cells at OCV.[29] Anyway, the data obtained by using symmetrical cells can be used qualitatively and could be useful to evaluate the effects of a polarization treatment on the electrode performance. The promotional effect of a polarization treatment was extensively studied on the widely used LSM cathode.[28,29,50–53] In the case of LSM–YSZ composite cathodes, its improved behavior after polarization has been attributed to several phenomena, such as (i) the reduction of Mn^{3+} in LSM with oxygen vacancies formation, providing sites for the O_2 activation,[54,55] (ii) the formation of microstructural changes, such as the formation of nanopores, that improve diffusion of oxygen species,[29,51,56] (iii) the reduction of the contribution of species that might passivate the TPB,[50,57] and (iv) the reduction of the interface between LSM and YSZ in the composite material, which prevent extensive formation of insulating $La_2Zr_2O_7$.[7,50]

All these effects could be active also in the polarization treatment of our LNF-based composite cathodes. We believe that, despite the nature of the electrolyte material, the main effects of the polarization treatments could be due to the partial reduction of the LNF with formation of oxygen vacancies and/or some microstructural modification with the formation of nanopores. Similar effects were also reported by Zhen et al.[58] and Orui et al.,[19] who attributed them to morphological changes, even if the mechanism of polarization enhancement is not still clear. As previously highlighted, ex situ XANES and EXAFS spectroscopies excluded the presence of appreciable oxygen vacancies in the starting material. Therefore, the current flow could result in the partial reduction of Ni(III) and/or Fe(III), with the formation of oxygen vacancies at least on the surface of the material and/or at the interface with the electrolyte. The increased number of oxygen vacancies promotes the overall O_2 reduction process. As evidenced by EIS measurements, after polarization the frequency related to the maximum of the arc moved to higher values (~2.5 kHz), which is commonly associated with a O_2 reduction process limited by the charge-transfer process. The formation of oxygen vacancies during the cathodic polarization treatment could promote the ionic diffusion through the LNF material and increase the number of sites for O_2 adsorption but probably does not affect significantly the electron transfer to the adsorbed O_2. Without excluding the eventual formation of nanopores, the partial reduction of LNF could result in a considerable extension of the TPB and a better performances of the composite electrode.

The deactivation observed after polarization as a result of a prolonged treatment at 700 °C (Figure 11) could be associated with progressive reoxidation of the reduced B ions. In fact, the progressive reaction with O_2 could lead to the filling of the oxygen vacancies with the loss of the active sites for O_2 adsorption and diffusion. Furthermore, the aging can lead also to modification of the TPB extension, resulting in the sintering of the nanopores formed during the polarization. As a consequence, the corresponding Nyquist plots appeared affected also by the contribution at lower frequencies related to diffusional processes.

Conclusions

The following main conclusions can be drawn from the present study on the preparation, characterization, and electrochemical properties of pure and composite LNF-based cathodes:

1. XAFS investigations of $LaNi_{0.6}Fe_{0.4}O_3$ (LNF) calcined at 1000 °C revealed that Fe and Ni are in the (III) oxidation state and that a negligible number of oxygen vacancies are present.

2. Consistently with literature data, LNF showed a diffuse solid-state reaction with YSZ, forming an insulating layer of $La_2Zr_2O_7$ also after calcination at 1000 °C for a short period (5 h). $LaNi_{0.6}Fe_{0.4}O_3$ was instead compatible with a SDC electrolytic material: no reaction between LNF and SDC was evidenced by XRD even after severe sinterization at 1100 °C.

3. The formation of $La_2Zr_2O_7$ has a detrimental effect on the performance of a composite LNF–YSZ electrode, leading to higher ASR value with respect to the system with pure LNF or composite LNF–SDC as electrode.

4. The observed high values for the activation energy of the cathodic process on LNF are consistent with a rate-determining step involving the O_2 activation and/or the diffusion of oxide ions.

(50) Jiang, S. P.; Love, J. G.; Zhang, J. P.; Hoang, M.; Ramprakash, Y.; Hughes, A. E.; Badwal, S. P. S. *Solid State Ionics* **1999**, *121*, 1–10.
(51) Jiang, S. P.; Love, J. G. *Solid State Ionics* **2003**, *158*, 45–53.
(52) Jiang, S. P.; Wang, W. *Solid State Ionics* **2005**, *176*, 1185–1191.
(53) Wang, W.; Jiang, S. P. *Solid State Ionics* **2006**, *177*, 1361–1369.
(54) Chen, X. J.; Chan, S. H.; Khor, K. A. *Solid State Ionics* **2003**, *164*, 17–25.
(55) Chen, X. J.; Khor, K. A.; Chan, S. H. *Solid State Ionics* **2004**, *167*, 379–387.
(56) Kuznecov, M.; Otschik, P.; Obenaus, P.; Eichler, K.; Schaffrath, W. *Solid State Ionics* **2003**, *157*, 371–378.
(57) Jiang, S. P.; Love, J. G. *Solid State Ionics* **2001**, *138*, 183–190.
(58) Zhen, Y. D.; Tok, A. I. Y.; Jiang, S. P.; Boey, F. Y. C. *J. Power Sources* **2007**, *170*, 61–66.

5. A cathodic polarization treatment strongly improves the performances of cathode using both SDC or YSZ as electrolyte.

Acknowledgment. Dr. G. Balducci (University of Trieste), Prof. P. Nanni and Prof. A. Barbucci (University of Genova), and Dr. Massimo Viviani (CNR-Genova) are acknowledged for useful discussions. Dr. L. Olivi (Synchrotron Elettra, Trieste) is acknowledged for the technical assistance in the XANES/EXAFS measurements. TOSOH is acknowledged for the providing of TS-8Y powder. University of Trieste, Centre of Excellence for Nanostructured Material, INSTM, Synchrotron Trieste, and FISR2002 "Nanosistemi inorganici ed ibridi per lo sviluppo e l'innovazione di celle a combustibile" are gratefully acknowledged for financial support.

CM071622N